El Niño as a mediator of the solar influence on climate

Julien Emile-Geay,[1,2] Mark Cane,[1] Richard Seager,[1] Alexey Kaplan,[1] and Peter Almasi[1]

[1] Using a climate model of intermediate complexity, we simulate the response of the El Niño−Southern Oscillation (ENSO) system to solar and orbital forcing over the Holocene. Solar forcing is reconstructed from radiocarbon production rate data, using various scaling factors to account for the conflicting estimates of solar irradiance variability. As estimates of the difference since the Maunder Minimum range from 0.05% to 0.5% of the solar "constant," we consider these two extreme scenarios, along with the intermediate case of 0.2%. We show that for large or moderate forcings, the low-pass-filtered east-west sea surface temperature gradient along the equator responds almost linearly to irradiance forcing, with a short phase lag (about a decade). Wavelet analysis shows a statistically significant enhancement of the century-to-millennial-scale ENSO variability for even a moderate irradiance forcing. In contrast, the 0.05% case displays no such enhancement. Orbitally driven insolation forcing is found to produce a long-term increase of ENSO variability from the early Holocene onward, in accordance with previous findings. When both forcings are combined, the superposition is approximately linear in the strong scaling case. Overall, the sea surface temperature response is of the magnitude required, and is persistent enough, to induce important climatic perturbations worldwide. The results suggest that ENSO may plausibly have acted as a mediator between the Sun and the Earth's climate. A comparison to key Holocene climate records, from the Northern Hemisphere subtropics and midlatitudes, shows support for this hypothesis.

1. Introduction

[2] The concept of a solar influence on the Earth's climate is hardly new. Sunspots were a favored explanation for monsoon failures as early as 1875 [see *Davis*, 2001, chapter 7], and the link between the Maunder Minimum and the Little Ice Age was made a century later [*Eddy*, 1977] (for recent reviews, see *Rind* [2002] and *Bard and Frank* [2006]). Since solar radiation is the primary source of energy driving atmospheric and oceanic flow, and since its intensity is thought to vary on long timescales (see *Fröhlich and Lean* [2004] for a review), it is often invoked to explain natural climate change on decadal [*van Loon and Labitzke*, 1988] to multicentennial timescales [e.g., *Jones and Mann* 2004]. The puzzling fact is that even generous reconstructions of past total irradiance changes do not yield changes bigger than 0.5% of the current solar irradiance (about 6.8 out of 1366 W m^{-2}) since the Maunder Minimum. The challenge is to understand how these subtle radiative fluctuations could emerge as a significant driving force of the Earth's climate, a system showing a considerable degree of internal variability.

[3] In a seminal paper, *Bond et al.* [2001] demonstrated an intriguing correlation between proxies of solar activity and the quantity of ice-rafted debris recorded at their coring of the northeastern North Atlantic (Denmark Strait and Feni Drift). *Bond et al.* [2001, p. 2130] concluded to a "persistent solar influence on North Atlantic climate during the Holocene." Prompted by their work, a number of investigators have attempted to understand this link. So far, the main dynamical pathway from the Sun to the surface has invoked the stratosphere and its effect on planetary wave propagation [e.g., *Geller and Alpert*, 1980; *Haigh*, 1996]. Fluctuations in the ultraviolet (UV) spectral band have been shown to alter stratospheric ozone photochemistry, and therefore latitudinal temperature gradients in the lower stratosphere. This translates into changes in the index of refraction of upward propagating planetary waves, which forces a redistribution of momentum fluxes in the upper troposphere, eventually leading to surface climate change, mainly over northern hemisphere continents [*Shindell et al.*, 1999]. A more recent account describes a mechanism with a very different premise, but with similar route through the stratosphere: *Shindell et al.* [2001] propose that with increased irradiance, tropical and subtropical sea surface temperatures (SSTs) increase, leading to a warmer tropical and subtropical upper troposphere via moist convection. This results in an increased latitudinal temperature gradient near the tropopause, again refracting upward propagating tropospheric planetary waves equatorward. The associated angular momentum transport produces changes in surface temperature and pressure corresponding to a high AO/NAO index. However, *Bond et al.* [2001] show that this can only partially explain their record.

[1]Lamont-Doherty Earth Observatory of Columbia University, Palisades, New York, USA.
[2]Now at Department of Earth and Atmospheric Sciences, Georgia Institute of Technology, Atlanta, Georgia, USA.

[4] In this paper we explore a new pathway of solar influence on climate, one centered around the El Niño–Southern Oscillation (ENSO) (that is to say, of purely tropical origin), and irrespective of the spectral signature of solar changes. Following *Mann et al.* [2005] and *Clement et al.* [1999], we employ a simplified model of the tropical Pacific atmosphere-ocean system [*Zebiak and Cane*, 1987] and diagnose its reaction to solar and orbital forcing over the past 10,000 years, in a variety of experiments. We show that even in the face of realistic amounts of weather noise, low-frequency solar irradiance fluctuations induce notable changes in the east-west temperature gradient, and in ENSO activity. The changes, albeit subtle, are of sufficient magnitude to produce sizable hydroclimatic impacts around the Pacific [*Seager et al.*, 2005b]. We show that this response can also generate substantial impacts worldwide, in particular over the North Atlantic, and submit this mechanism as an explanation for the key paleoclimate records documenting the Sun-climate relationship over the Holocene.

2. Climate Forcing Over the Holocene

[5] Given our model's formulation in terms of anomalies (see section 3), the climate forcings of interest are departures from the current radiative budget. First, one has to consider fluctuations in solar forcing arising from the changes in the Earth's orbit ("orbital forcing"), as in the work by *Clement et al.* [1999]. Second, changes in the actual solar irradiance need to be accounted for ("solar forcing"). Third, one should include the effect of volcanic aerosol loading in the lower stratosphere, which has been suggested to account for some important SST anomalies in the tropical Pacific over the past millennium [*Mann et al.*, 2005]. Unfortunately, such a data set is currently unavailable over the entire Holocene. The present study will therefore ignore this effect, with the recognition that a thorough analysis must include tropical volcanic forcing when such data becomes available.

2.1. Orbital Forcing

[6] The orbital forcing is well known, and can be readily and accurately computed [*Berger*, 1978]. In order to separate the effect of various orbital motions, we carry out an empirical orthogonal function (EOF) decomposition of insolation as a function of calendar month, latitude and year. Nevertheless, the forcing applied to the model is the total departure from current insolation computed via *Berger*'s [1978] code, without EOF truncation. The latitude grid is restricted to the tropical band [29°S; 29°N], and the time grid spans 1 million years, necessary to cleanly isolate important orbital periodicities.

[7] In Figure 1 we show the first three EOFs (accounting for 99.7% of the variance over the Holocene), the associated principal components (PCs) and their spectral density. The first two EOFs are clearly associated with precession, with a peak at a period of 23 kyr, zero annual mean and weak dependence on latitude. EOF1 is associated with the summertime/wintertime insolation contrast near the equator. Similarly, EOF2 can be described as the spring-fall insolation contrast at the equator. Although the two PCs are, by construction, orthogonal over the last million years, they

are significantly correlated ($\rho \sim 0.5$) over the Holocene. The third EOF is associated with obliquity changes, with a period of 43 kyr, and the two hemispheres out of phase. Although it only accounts for 0.84% of the overall variance, the annual mean contribution of obliquity is nonzero, in contrast to precession. Indeed, these changes are mostly responsible for the increase of ~ 1 W m^{-2} at the equator since the early Holocene (changes in eccentricity are negligible). Overall, these three EOFs show that the northern hemisphere summer-winter contrast has kept decreasing since the early Holocene, and so has the fall-spring contrast since about 5000 B.P, while the annual mean has slowly kept rising.

2.2. Solar Irradiance Forcing

[8] As emphasized in the Introduction, reconstructions of past solar irradiance variations are a matter of considerable debate and vexingly large uncertainties. The reconstructions rely on sunspot observations for recent centuries, and on paleoproxy records of cosmogenic nuclides (^{14}C, ^{10}Be, ^{36}Cl) for the longer record. The latter are directly influenced by changes in magnetic flux from the Sun, not changes in irradiance. A relationship between the two must be created by extrapolating from the short record of radiometric measurements, inferring a low-frequency irradiance component from observations of the group sunspot number gathered since the invention of the telescope [see *Fröhlich and Lean*, 2004, and references therein]. There is no obvious way to perform this extrapolation.

[9] By consistency with *Bond et al.* [2001], we use the detrended ^{14}C production rate (from INTCAL98 [*Stuiver et al.*, 1998]) as a proxy for solar activity, after applying a 40-year low-pass filter to remove high-frequency fluctuations, which makes the scaling more meaningful (these periods are too short to affect our model). In Figure 2 we show the forcing and an estimate of its spectrum. The record clearly contains the documented centennial variability of the Gleissberg (~ 88 years) and DeVries (~ 205 years) cycles [*Peristykh and Damon*, 2003; *Wagner et al.*, 2001], as well as significant power around 500 years, and a broad band around 1000 years. These centennial- to millennial-scale fluctuations are also present in several records of ^{10}Be accumulation (not shown), so that confidence can be gained that both nuclides were recording production-related changes. Indeed, Be and C have such different geochemical cycles that their coherent behavior must not reflect climate effects but a common external source: nuclide production. For periods shorter than about 3000 years (but longer than a few decades), it is a fair assumption to neglect changes in the geomagnetic field, and changes in production are commonly attributed to the Sun's magnetic activity [*Bard et al.*, 2000; *Muscheler et al.*, 2006]. Nonetheless, the existence of millennial solar cycles is not firmly established [*Marchal*, 2005; *Saint-Onge et al.*, 2003], and some of our results rest on the assumption that they are real.

[10] There remains the problem of translating the loosely defined "solar activity" into irradiance. Though sophisticated techniques have been applied to this end [*Mordvinov et al.*, 2004], no such reconstruction is available for the Holocene at the time of publication. We therefore apply the linear scaling of *Bard et al.* [2000]: The reference scale
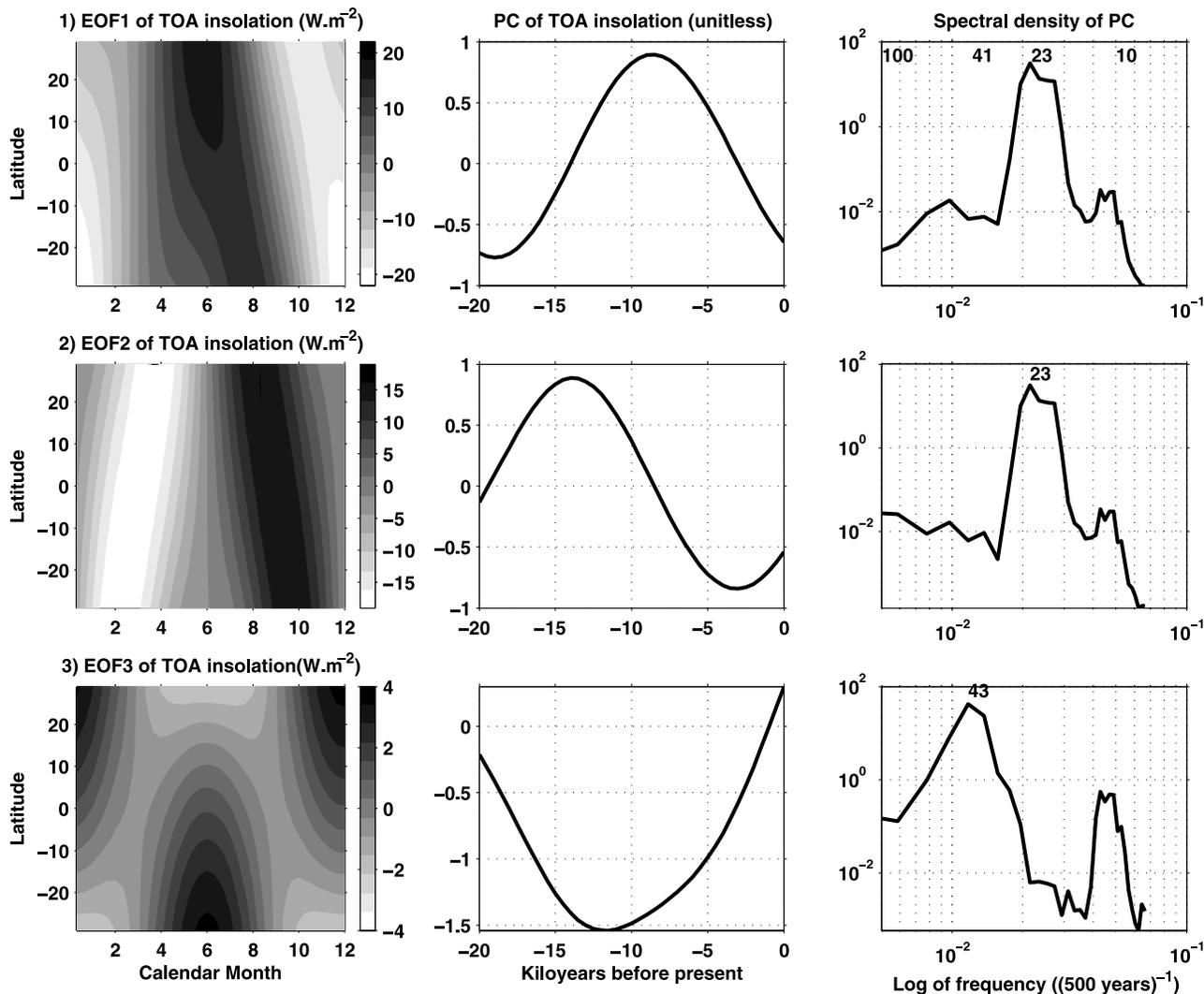
Figure 1. EOF analysis of the top-of-the-atmosphere insolation over the Holocene. (left) EOF pattern as a function of calendar month (January = 1, February = 2, March = 3), (middle) PC time series, and (right) its spectral density, computed with the multitaper method [*Thomson*, 1982]. Numbers above the graph refer to the period in kyr. To obtain the contribution of a mode to the total insolation at any given time, each EOF pattern must be weighted by the value of the corresponding PC.

(ΔF) here is the difference in TSI/4 (total solar irradiance, divided by 4 because of spherical geometry) from the Maunder Minimum (roughly 1645 to 1715 A.D.) to the "present" (1950 A.D.). It is essentially the sunspot number difference multiplied by the slope of the scatterplot of irradiance versus sunspot number. The latter, as discussed above, is only based on about 20 years of reliable radiometric data. Since published estimates of the difference [*Fröhlich and Lean*, 2004] range from $\Delta F = 0.05\%$ to 0.5% of the solar "constant" ($S_\circ = 1366$ W m^{-2} for consistency with *Berger* [1978]), we consider these two extreme cases, along with the intermediate case of 0.2%, corresponding to peak-to-peak differences of, respectively, 0.17, 0.68 and 1.7 W m^{-2}. The 0.2% case is close to the value used by *Crowley* [2000] and *Weber et al.* [2004]. It is

worth emphasizing that most recent estimates are on the lower end of this interval [*Foukal et al.*, 2006; *Fröhlich and Lean*, 2004], though the solar physics community is far from having reached a consensus on the issue. Also, these long-term changes are thought to have a marked maximum in the UV domain, but recent GCM experiments show that the atmosphere's response is somewhat indifferent to the spectral signature of the forcing [*Rind et al.*, 2004].

3. Experimental Setting

3.1. The Model

[11] We use the intermediate-complexity model of *Zebiak and Cane* [1987]. It is a model with linear shallow water dynamics for the global atmosphere [*Gill*, 1980; *Zebiak*, 1982] and the tropical Pacific Ocean [*Cane and Patton*,
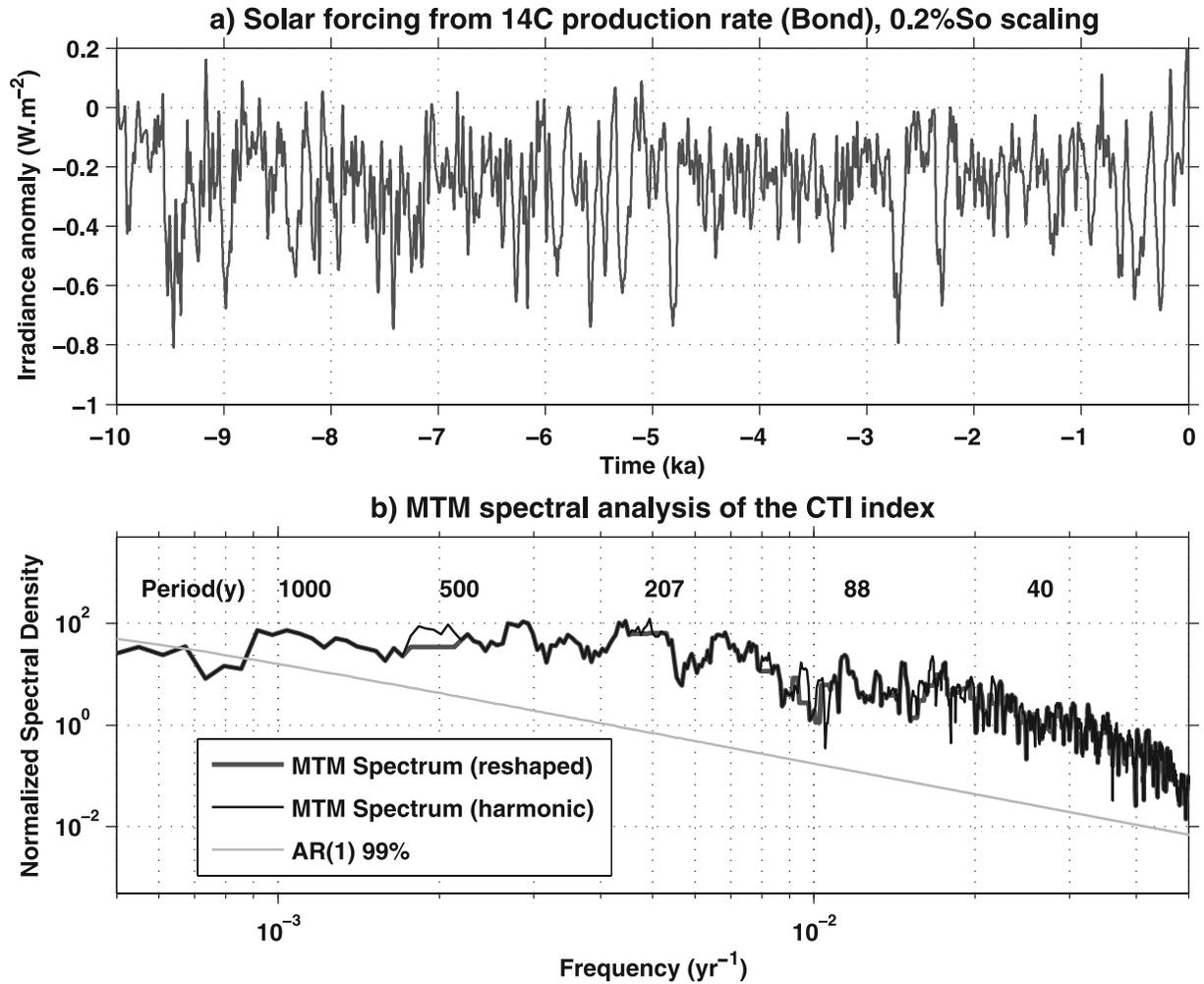
Figure 2. Spectral analysis of the ^{14}C production rate record. (a) The ^{14}C time series from *Bond et al.* [2001], converted to W m^{−2} for the intermediate scaling: a Maunder Minimum solar dimming of $0.2\% \times S_o$ (see text for details). (b) Multitaper spectra and 99% confidence level for rejecting the null hypothesis that the series is pure "red noise" (AR(1) process). This follows the methodology of *Mann and Lees* [1996].

1984], coupled by nonlinear thermodynamics, which give the model self-sustained ENSO variability. The ocean model domain is restricted to [124°E−80°SW; 29°S−29°N], which means that only tropical processes are considered. The model is linearized around a constant climatology [*Rasmussen and Carpenter*, 1982].

[12] We employ the same configuration as *Clement et al.* [1999], in the model version written by T. Kagimoto at the International Research Institute for Climate Prediction. Radiative forcing anomalies are included as a source term of the (prognostic) equation for sea surface temperature (SST). Conversion is made from the top-of-the-atmosphere perturbation to a surface flux by multiplying by $(1 − 0.62C + 0.0019\,\alpha)$, where C is the cloud fraction and α is the noon solar altitude [*Reed*, 1977]. Consistent with the absence of radiative scheme in the model, we hold the cloud fraction constant, 50%. As in the work by *Mann et al.* [2005], the

solar forcing estimates are multiplied by a factor of $\pi/2$, since the model represents only the Tropics.

3.2. Representation of Weather Noise

[13] The tropical Pacific ocean-atmosphere system is the stage of considerable interannual and intraseasonal variability. Whether one is the child of the other is a question beyond the scope of this paper. The question relevant to the present study is whether the ENSO system would notice solar irradiance perturbations in the presence of a physically realistic amount of weather noise. The latter concept encompasses all wind fluctuations that are external to the coupled subsystem, which our model is designed to represent. The simplest way to parameterize this phenomenon is to model it as a uniform patch of westerlies over the western equatorial Pacific (hereafter WP, spanning [165°E−195°SE, 5°S−5°S]). Its behavior in time can be described by a statistical model that crudely approximates the low-order moments of the observed zonal wind stress (τ_x). An

Table 1. Summary of the Numerical Experiments Used in This Study

Set	Scale	Noise Level	Name
Solar	0.5	40%	Sol0.5
	0.2	40%	Sol0.2
	0.05	40%, 0%	Sol0.05
Orbital	NA	40%, 0%	Orb
Orbital and solar	0.5	40%	Orb_Sol_0.5
	0.2	40%	Orb_Sol_0.2

autoregressive model of order 1 [AR(1)] seems appropriate for such a process. The amplitude of this random wind forcing (its time-integrated variance σ_N^2) can be defined as the fraction of monthly τ_x variability that is not accounted for by a direct response to SST forcing: $\sigma_N = \ell \, \sigma_{NCEP}$, where σ_{NCEP} is the observed monthly wind stress in the NCEP reanalysis [*Kalnay et al.*, 1996].

[14] Multimember ensemble experiments with a state-of-the-art coupled ocean-atmosphere general circulation model (OAGCM) suggest that $\ell \simeq 40\%$ (A. Wittenberg, personal communication, 2005), corresponding to a noise variance of 16% of the total. The AR(1) parameter is the lag 1 autocorrelation of monthly τ_x over the WP, estimated from NCEP data at $\alpha = 0.73$.

[15] The AR(1) processes $X(t)$ are generated numerically, and the wind noise $\tau_x^N(t) = \ell \, X(t)$ is then applied uniformly onto the WP box for the whole length of the simulation.

[16] In Table 1 we summarize the different numerical experiments conducted in this study.

4. Results

4.1. Solar

[17] In the following, our diagnostic variable of choice is the ensemble mean zonal SST gradient along the equator (EW), which is the difference between the WP index (average SST over the aforementioned western Pacific box) and the NINO3 index (average SST over [150°E–90°W, 5°S–5°N]). This procedure removes any zonally uniform temperature change and reduces the noise significantly. A positive EW means that the gradient is strengthened, indicative of La Niña-like conditions.

[18] In Figure 3 we present the results of the model forced by reconstructed solar irradiance ($\Delta F = 0.2\% S_o$), in a six-member ensemble. As is apparent from Figure 3a, the 40-year low-passed EW responds almost linearly to the irradiance forcing, with an amplitude of 0.3°C. While this may look insignificant at first sight, recent research on the origin of North American drought has demonstrated, using two different general circulation models, that La Niña-like anomalies of such amplitude generated the sequence of

severe droughts that visited the American West since the midnineteenth century, including the 1930s [*Schubert et al.*, 2004; *Seager et al.*, 2005b; *Herweijer et al.*, 2006]. SST variations this small, if persistent enough, are sufficient to alter extratropical atmospheric circulation and perturb local hydroclimates in the western United States, South America, and elsewhere [*Herweijer and Seager*, 2007].

[19] Figure 3b shows the wavelet spectral density of the same EW index, which is a convenient way of visualizing the evolution of a power spectrum through time. Its application to climate time series has been developed by *Torrence and Compo* [1998]. Though nonstationary, the signal generally shows the highest power in the ENSO band (2 to 7 year period, centered around 4 years) and the centennial to millennial band (~200 to 1000 years) where the solar forcing displays its maximum variance. However, variability in this band could be entirely due to the model's internal chaotic dynamics, as shown by *Clement et al.* [1999]. We therefore devise the following test: From a 150,000 yearlong unforced run of the model, we extract 400 time series of the same length as the simulations of interest (i.e., 10,000 years), with starting times picked at random more than 100 years apart. We perform the wavelet analysis on each of those time series, compute their global wavelet spectrum and for each scale, sort the spectra in increasing order. The upper 20 thus define the 95% confidence level.

[20] From this we can see on Figure 3c that only in the 500 and 1000 year bands does the model response exceed its level of natural variability at the 95% level. Interestingly, the model internal variability does exhibit a weak peak in the millennial band, though it knows of no numerical constant or physical process that could have introduced such a timescale. It is an illustration that the nonlinear atmosphere/ocean feedbacks it embodies can generate variability at unexpectedly long periods. The fact that it also responds to forcing at such frequencies could be perceived as a form of damped resonance, but this is not the case: Perturbing the model by a white noise radiative forcing with the same variance as the $\Delta F = 0.2\% S_o$ case, we find that variability is raised uniformly at all frequencies and that the millennial scale is not favored.

[21] Note that this approach implicitly assumes that the time series extracted from the unforced run are statistically independent, which may seem contradictory, as they are part of the same realization of a numerical dynamical system. We assert that independence is true for all practical purposes, as predictability studies with the same model [e.g., *Karspeck et al.* 2004] show that its NINO3 index is of very limited predictability even a decade or two in advance.

[22] Why does the model respond with increased SST gradient to positive radiative forcing? This may be understood as follows [*Clement et al.*, 1996]: If there is heating over the entire tropics, then the Pacific will warm more in

Figure 3. Model response to solar forcing ($\Delta F = 0.2\% S_o$, experiment Sol0.2). (a) Solar forcing (grey) and response ($T_W - T_E$) (black). (b) Wavelet spectral density (arbitrary units, with maxima in black, minima in white). The thick black line is the cone of influence, the region under which boundary effects can no longer be ignored [*Torrence and Compo*, 1998]. The Morlet wavelet was used here). (c) Global wavelet spectrum and 95% confidence level (see text for details). (d) Probability of a large El Niño event over a 200-year window.
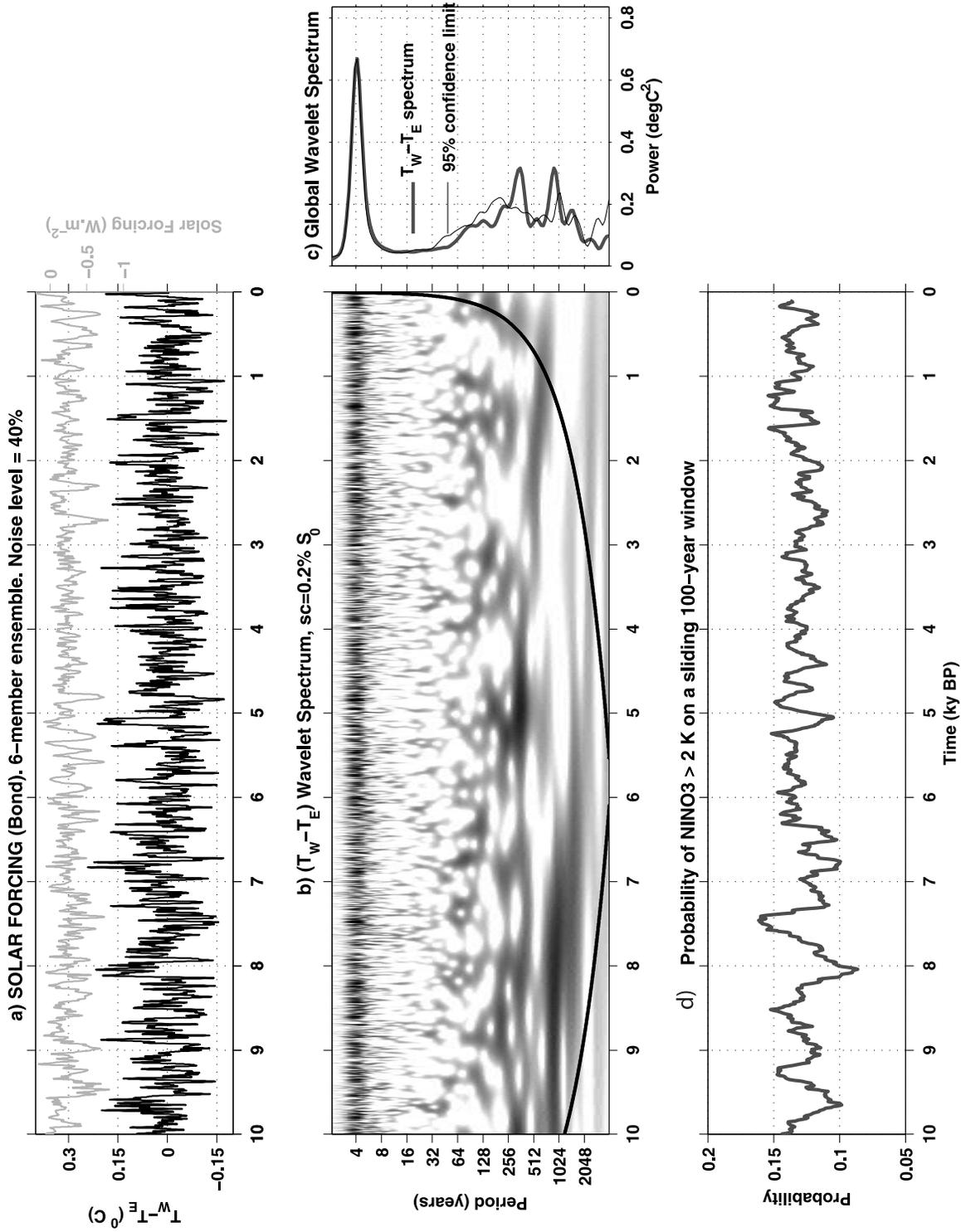
Figure 3

the west than in the east because the strong upwelling and surface divergence in the east moves some of the heat poleward. Hence the east-west temperature gradient will strengthen, causing easterly winds to intensify, further enhancing the zonal temperature gradient (the *Bjerknes* [1969] feedback). This process leads to a more La Niña-like state (positive values of the EW index) in response to increased irradiance. Such an adjustment typically occurs over a few years to a decade, so that on millennial time-scales, it looks virtually instantaneous. The dynamical feedback that makes the SST harder to change in the east has earned the name "thermostat" to this mechanism. Quantitatively, we find the intermediate scaling ($\Delta F = 0.2\% S_o$) sufficient to trigger these feedbacks, while the weaker one ($\Delta F = 0.05\% S_o$) is not: At least in our model, a forcing that small would not generate a noticeable response.

[23] Finally, we present in Figure 3d the probability of a strong El Niño event (NINO3 > 2 K for a year) on a 200-year window, as a measure of ENSO variability per se. Indeed, this quantity is more closely related to rainfall proxies from central and South America [e.g., *Moy et al.*, 2002; *Rein et al.*, 2004]. The index does show centennial to millennial cycles, but no obvious trend, unlike the orbitally forced model, as we shall see. Not surprisingly, it is significantly anticorrelated with EW, since the latter is equal to WP-NINO3, with WP exhibiting much weaker variations than NINO3. In turn, periods of higher NINO3 are synonymous with an increased likelihood of large ENSO events.

4.2. Orbital

[24] In Figure 4 we show the same quantities as before, in the case of the orbitally forced run. High wavelet spectral density is expected at orbital timescales, but its exact value is unreliable in this calculation, as it mostly lies within the "cone of influence" [*Torrence and Compo*, 1998]. Notice the small centennial-to-millennial power in this case, in contrast to the solar case.

[25] The salient feature is the growing intensity of ENSO activity from the mid-Holocene onward, which can be seen either in the wavelet spectrum (b) or the probability of large ENSO events (d). The latter features a prominent upward trend, with the probability of a strong El Niño gaining 50% over the Holocene. A similar finding was noted by *Clement et al.* [2000] and qualitatively supported by a flood proxy from Lake Pallcacocha [*Moy et al.*, 2002], high-resolution coral $\delta^{18}O$ from the Huon Peninsula [*Tudhope et al.*, 2001], and oxygen isotopes in deep-sea sediment cores from the ENSO source region [*Koutavas et al.*, 2006].

[26] The dynamical explanation for why ENSO has a low variance at times of stronger seasonality is given by *Clement et al.* [1999]. The reason is that the seasonal migration of the intertropical convergence zone (ITCZ) modulates the effective coupling strength [*Zebiak and Cane*, 1987], so that the system is most responsive to radiative anomalies centered around August/September: An increased insolation at that time of the year is then translated as a cooling in the eastern equatorial Pacific via the "thermostat" mechanism described above. This tends to suppress

the growth of large El Niño events at times where the summertime insolation was much stronger than now, such as the early Holocene. As this seasonal contrast wanes over the course of the Holocene, ENSO variance steadily grows toward modern-day values.

4.3. Orbital and Solar

[27] We now consider the model response when solar and orbital forcing act together. In this we neglect the interaction between solar and orbital forcing anomalies, i.e., the modulation of irradiance perturbations exerted by the departure from today's orbital configuration, since the product is too small to be of significance. The total radiative forcing is therefore, to a very good approximation, the sum of the two previously applied forcings (solar plus orbital).

[28] The model response is presented in Figure 5, with the same conventions as before, but with $\Delta F = 0.5\% S_o$. The overall result, clearly visible in Figure 5d is that both effects (slow orbital growth over the Holocene, important solar-induced variance at 500–1000 year scales) are superimposed, yet the model response is nonlinear. With a weaker $\Delta F = 0.2\% S_o$, the model produces centennial and millennial changes that are not quite large enough to pass the same significance test. They are, however, still visible in the probability of strong events, albeit weaker. This is because in the early part of the Holocene, orbital forcing weakens the effective air-sea coupling (as discussed above), which makes it harder for solar forcing to excite a thermostat type of response. Solar variability at centennial to millennial scales is thus subdued in this early part of the record, and only emerges in the second half of the Holocene.

[29] It is noteworthy that although solar forcing has peak-to-peak variations of $\sim$2 W m^{-2} even in the strong scaling case, much smaller than the summer-winter insolation difference (peaking at $\sim$40 W m^{-2}), their effect is disproportionately large: EW temperature responses are of similar amplitude for the two forcings. This is because the annual mean signal in insolation is of the same order as the solar forcing perturbation, about 1 W m^{-2}.

[30] How much of the ENSO variability can be linearly predicted from knowledge of solar irradiance and the Earth's orbital parameters? We consider the 6 realizations of the Orb_Sol_0.5 experiment, and perform a multivariate regression of the smoothed, ensemble mean EW time series over three variables: PC_1 and PC_2 from the EOF analysis presented in Figure 1 and the solar irradiance F_o from Figure 2. The EW gradient was low-pass-filtered at periods longer than 40 years with a Gaussian window prior to normalization, to ease comparison with Figures 3a, 4a, and 5a. Figure 6 (top) shows the result for the dependent variable and its predictors, and Figure 6 (bottom) shows the result of the regression.

[31] The linear correlation coefficient between predicted and "observed" time series is high ($\rho \simeq 0.70$). Such a correlation means that about half the time series variance can be explained by the linear response to the forcing, with orbital forcing accounting for 14% and irradiance fluctuations for 35%. This ratio does change qualitatively over a wide range of cutoff frequencies, since, as expected, the higher the cutoff, the lesser the fraction of variance
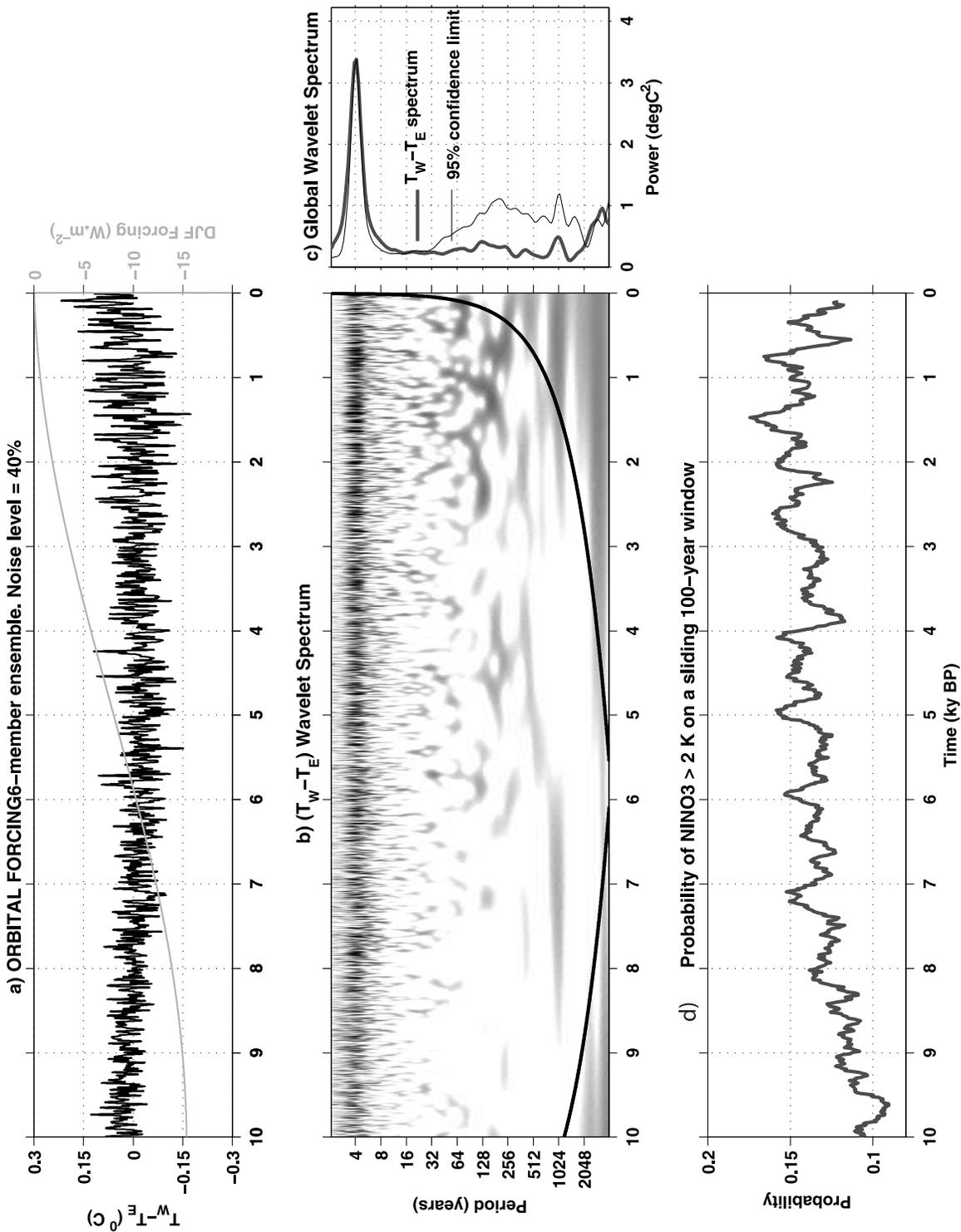
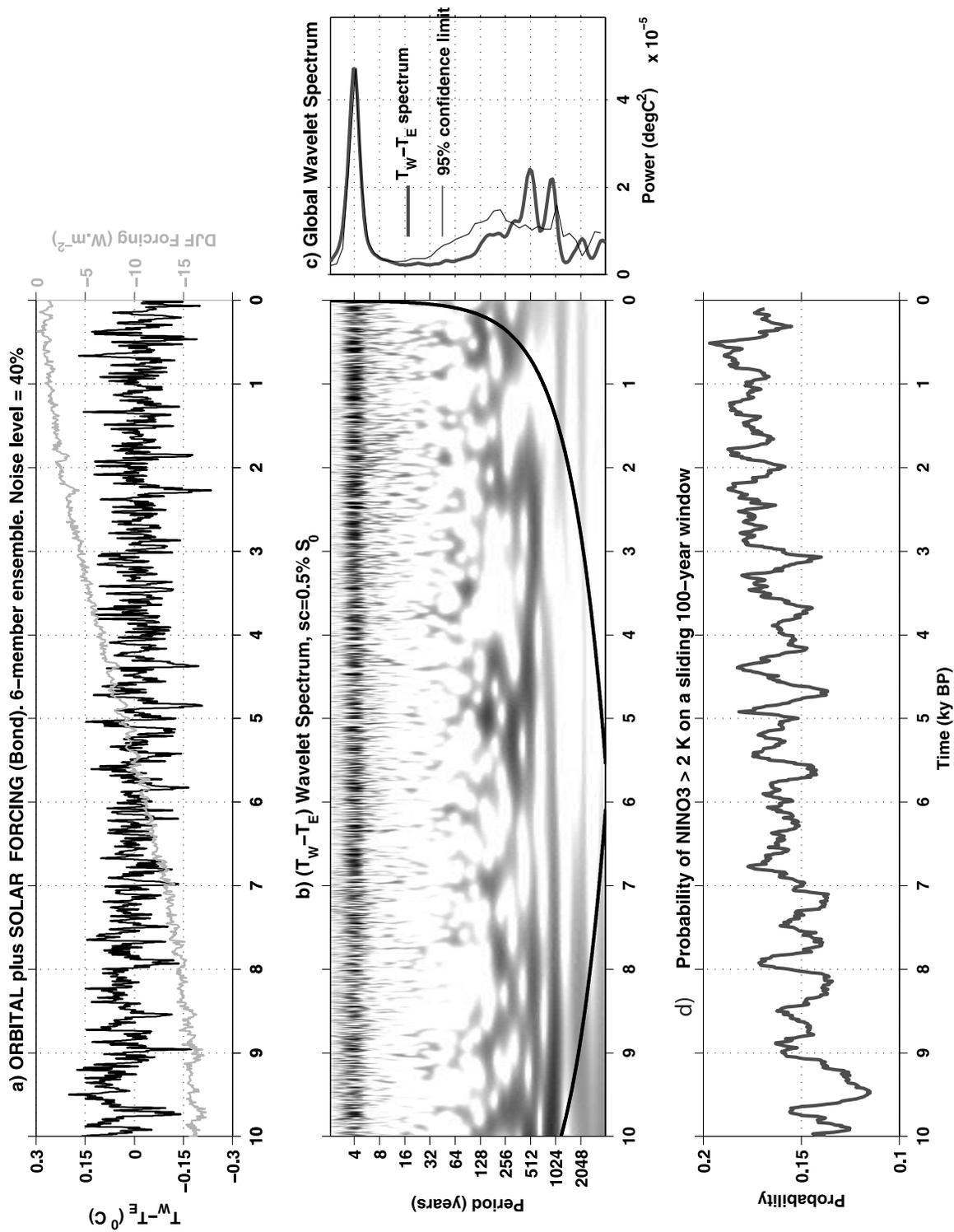**Figure 4.** Same as Figure 3 but for orbital forcing (experiment Orb).

Figure 5. Same as Figure 3 but with orbital and solar forcing ($\Delta F = 0.5\% S_o$, experiment Orb_Sol_0.5).
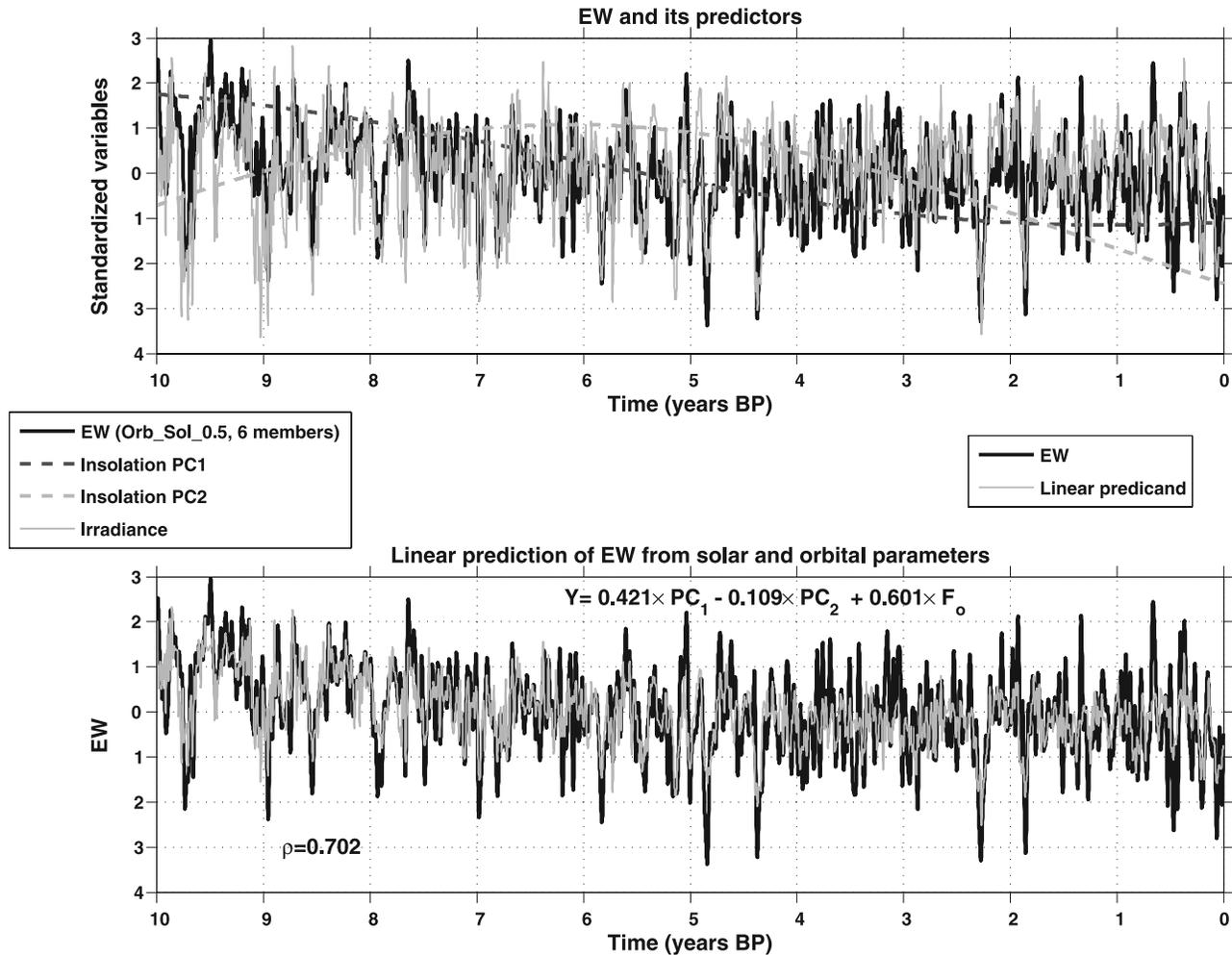
Figure 6. Linear prediction of ENSO variability from solar parameters. (top) Low-pass-filtered zonal SST difference (EW), and predictor variables: PC_1 and PC_2 from Figure 1 and F_o from Figure 2, with $\Delta F = 0.5\%S_o$ (bottom) Comparison between predicand and predicted variable. See text for details.

explained by the relatively small scales characteristic of solar forcing. What if the latter was weaker? With $\Delta F = 0.2\%S_o$, ρ drops to 0.51 ($\rho^2 = 26\%$). In that case the orbital part is nearly the same (12%), while the solar part is reduced to 14%, proportional to the reduction in irradiance.

[32] We conclude that in our model, solar perturbations of midrange amplitude are sufficient to generate persistent SST anomalies of a fraction of a degree on millennial timescales, via the thermostat mechanism, reflected in the likelihood of strong El Niño events. Hence ENSO may have acted as a recipient and transmitter of solar influence. The question is could such changes influence other parts of the globe and is the global paleoclimate record consistent with this idea?

5. Global Implications

[33] We turn to the paleoclimate record to test the idea of a solar-induced "thermostat." *Mann et al.* [2005] show that their result is consistent with the Palmyra ENSO record of *Cobb et al.* [2003]: At times of increased irradiance, such as the Medieval Warm Period (900–1300 A.D.), the average

conditions were colder in the eastern equatorial Pacific (La Niña-like). Conversely, they were comparatively warmer (El Niño-like) during the Little Ice Age (1600–1850 A.D.), when solar irradiance was weaker. Does this relationship extend throughout the Holocene and is it consistent with climate signals in remote regions?

5.1. Solar-Induced ENSO and North America

[34] North America is one of the regions of the world with the strongest teleconnection pattern to the tropical Pacific. The same drought patterns linked to tropical Pacific SSTs in the instrumental period are also found in tree ring reconstructions of Palmer Drought Severity Index from the North American Drought Atlas for the medieval climate anomaly and Little Ice Age [*Cook et al.*, 2004, 2007]. *Herweijer et al.* [2007] review additional evidence for a La Niña-like global hydroclimate during the medieval climate anomaly.

[35] Consistent with our result, recent data by *Asmerom et al.* [2007] support the notion of an anticorrelation between solar activity (tree ring Δ^{14}C) and oxygen isotopic composition of uranium-series-dated speleothems in the American

southwest, taken as a proxy for ENSO-related precipitation over the entire course of the Holocene. Given that the model only predicts the ensemble average SST gradient to closely follow the forcing and that volcanic perturbations are absent from the latter, one would not expect the single realization provided by nature to match it exactly. On the contrary, the observed correspondence is unexpectedly high.

5.2. Solar-Induced ENSO and the North Atlantic

[36] We now go back to the original observation that motivated this work, and ask whether this theory can explain the Holocene record of ice-rafted debris (IRD) in the North Atlantic [*Bond et al.*, 2001]. They argue that synchronous increases in percentages of particular IRD grain types from three sites in the North Atlantic demonstrated not only basin-wide cooling, but changes in atmospheric and oceanic circulation [see also *Bond*, 2005]. Hematite-stained quartz grains, for example, must have been advected directly south of Iceland to produce the record at Feni Drift, an ice transport pattern inconsistent with a strong modern Icelandic Low centered near the Greenland-Faeroes ridge. This is in contradiction with the negative NAO pattern required by previous theories of Sun-induced climate change [*Shindell et al.*, 1999, 2001, 2003]. In contrast, we propose here that a wind pattern consistent with such ice drift can be driven from the tropics.

[37] The idea that Indo-Pacific SSTs can alter the climate of the North Atlantic was recently advanced by *Hoerling et al.* [2001], who used an atmospheric general circulation model (GCM) forced by historical SSTs in various basins (namely, the whole globe (GOGA) or solely the Tropics (TOGA)). They attributed the late twentieth century upward trend of the North Atlantic Oscillation (NAO) to the SST warming trend of the western equatorial Pacific and Indian Oceans, most likely due to anthropogenic greenhouse forcing. Accordingly, in our theory, increased solar irradiance would warm the western equatorial Pacific more than the east, which on these grounds would then be expected to push the NAO into a more positive phase.

[38] The search for stable correlations between the tropical Pacific and the North Atlantic has long been elusive [e.g., *Rogers*, 1984], but recent studies appear to capture them. Longer records have allowed such teleconnections to be established with instrumental data, also documenting them in several atmosphere models [*Toniazzo and Scaife*, 2006; *Brönnimann et al.*, 2007; *Bulic and Brankovic*, 2006]. Here we document the association of northerly winds over the northern North Atlantic with El Niño-like states of the tropical Pacific, which we diagnose in the extended instrumental record and explain via state-of-the-art climate models. The details of the procedure are given in Appendix A, and the result is shown in Figure 7. It can be seen that all three data sets concur to show that ENSO states tend to coincide with northeasterly winds over the Fram and Denmark straits, with a pattern broadly reminiscent of (but not identical to) a negative NAO. This is consistent with the work by *Toniazzo and Scaife* [2006] and *Brönnimann et al.* [2004].

[39] We note that the changes shown here are of subtle magnitude, and may be an imperfect analog to millennial

changes relevant to the interpretation of the IRD record. Nevertheless, they hint at the possibility that ENSO may be driving surface ocean circulation over the North Atlantic, in the direction required to produce IRD discharge events. It is likely that feedbacks must be invoked to generate a more sizable response: The ENSO-induced southwestward winds at high latitudes would cool the North Atlantic and trigger a southward ice drift, which would also lower the local sea surface salinity. This would weaken the buoyancy-driven circulation and its associated heat transport, further cooling the area. Recent modeling experiments [*Vellinga and Wood*, 2002; *Chiang et al.*, 2003; *Zhang and Delworth*, 2005] have suggested that such SST anomalies in the Atlantic would shift the Pacific intertropical convergence zone southward, reducing the mean SST gradient along the equator, which would further intensify the El Niño-like anomaly. Thus it is plausible that such ENSO-induced perturbation in the North Atlantic would reverberate back into the tropical Pacific: a positive feedback. The important idea is that solar forcing, weak though it is, is persistent enough to seed these changes into the Tropics, from which they can be exported to high latitudes, and further amplified by feedbacks involving sea ice and the thermohaline circulation. Though much work remains to be done to establish a quantitative relationship between tropical climate and ice rafting in the North Atlantic, we have outlined here a physical mechanism that could account for such a link.

5.3. Solar-Induced ENSO and the Monsoons

[40] Numerous studies have shown a significant simultaneous association between El Niño and weaker monsoon rainfall over India and southeast Asia [e.g., *Pant and Parthasarathy*, 1981; *Rasmussen and Carpenter*, 1983; *Ropelewski and Halpert*, 1987]. It is therefore natural to expect persistent anomalies of eastern Pacific SST to have a noticeable influence on the Indian and Asian monsoons, though this could possibly involve a feedback between the two oscillations [*Chung and Nigam*, 1999].

[41] The activity of these monsoons has been documented on a broad range of timescales, and recently been tied to abrupt climate change in the North Atlantic [*Vellinga and Wood*, 2002; *Zhang and Delworth*, 2005]. Speleothem records from northern Oman [*Neff et al.*, 2001], southern Oman [*Fleitmann et al.*, 2003], the Chinese cave of Dongge [*Wang et al.*, 2005], and anoxic sediments off the coast of Oman [*Gupta et al.*, 2003], converge to a coherent depiction of the Indian and Asian monsoons: In all these records, there is a millennial-scale correlation of weaker monsoons with IRD deposits in the North Atlantic [*Bond et al.*, 2001]. This is consistent with periods of lower irradiance inducing an El Niño-like response.

6. Discussion

6.1. Summary

[42] We have found that solar and orbital forcing combine in a way that produces ENSO-like variance at centennial-to-millennial timescales, well above the model's level of internal variability. The physics of the ocean-atmosphere system embodied in the model are able to pick out solar irradiance perturbations of intermediate amplitude ($\Delta F =$
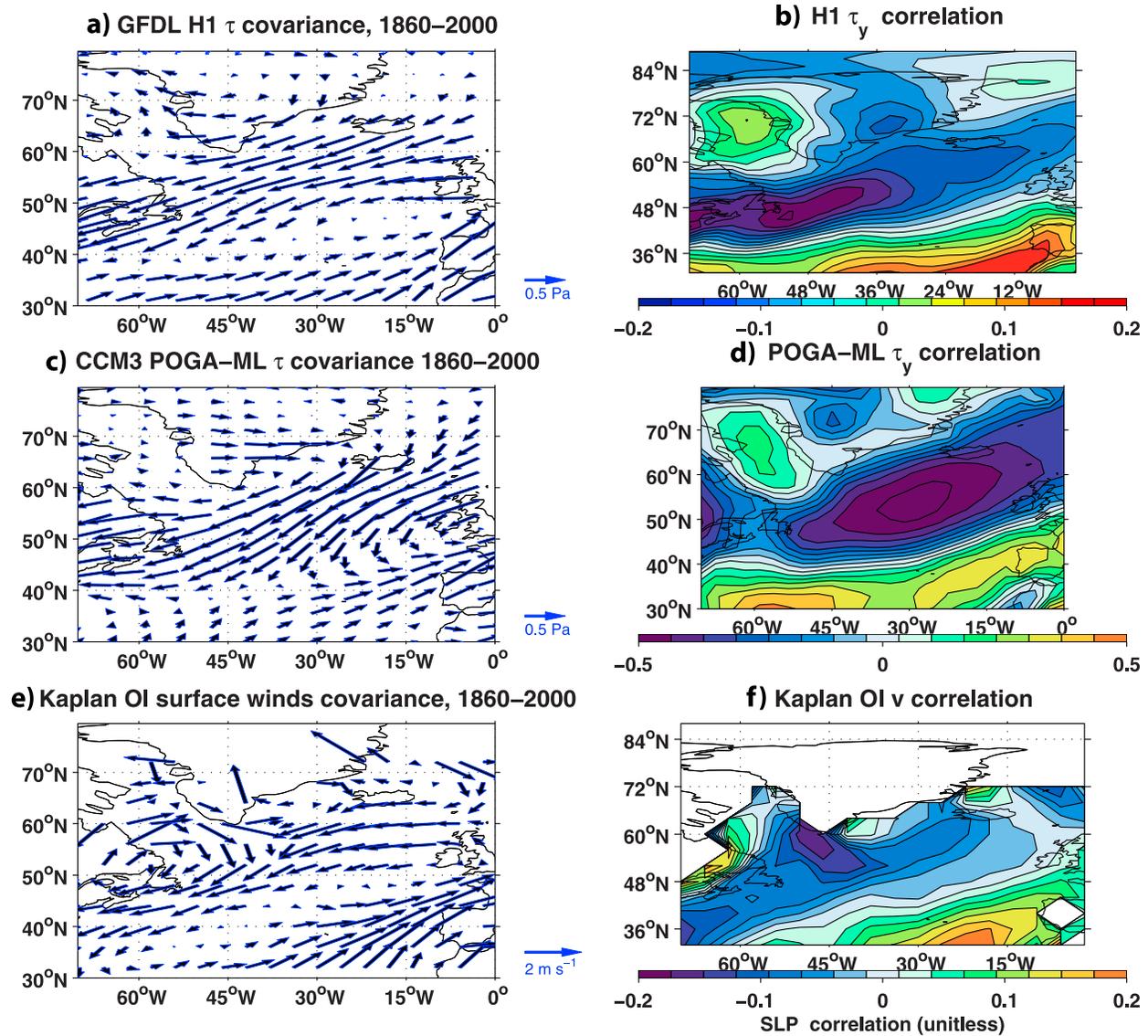
Figure 7. ENSO influence over the North Atlantic. (left) Regression patterns of wind vectors from the specified product, smoothed by a 3-month running average, on the NINO3 index, normalized to unit variance. Hence units of regression coefficients are given per standard deviation of the index. (right) Corresponding correlation patterns, shown for the meridional component only. (a) GFDL H1 surface wind stress regression. (b) GFDL H1 meridional wind stress correlation. (c) POGA-ML surface wind stress regression. (d) POGA-ML meridional wind stress correlation. (e) Analysis of ICOADS data, surface wind regression. (f) Analysis of ICOADS data, meridional wind correlation.

$0.2\%S_o$), in the presence of orbital forcing and, remarkably, in all cases, in the presence of a realistic amount of weather noise. For weak scalings of the solar irradiance ($\Delta F = 0.05\%S_o$), however, the response is indistinguishable from the variability of the unforced system. The results confirm the importance of orbital forcing in creating conditions favorable to the growth of ENSO variance over the Holocene, and suggest that solar irradiance variability may add centennial-to-millennial-scale ENSO variance.

[43] We find qualitative agreement with high-resolution paleoclimate data and propose that ENSO mediated the

response to changes in solar activity discovered in climate proxies around the world.

6.2. Limitations of the Model Arrangement

[44] The simplicity of the model is what allows the study of the coupled system over such long timescales, yet it creates caveats that are inherent to the model's formulation [*Clement et al.*, 1999]. While the chain of physical reasoning linking solar forcing to equatorial SSTs (the thermostat mechanism) is certainly correct as far as it goes, the climate system is complex and processes not considered in this

argument might be important. Perhaps cloud feedbacks play a substantial role, although it is still unknown whether the feedbacks associated with solar forcing would be positive or negative [*Rind*, 2002]. In a time of enhanced solar heating, the oceans should generally warm everywhere, including the subduction zones of the waters which ultimately make up the equatorial thermocline [*McCreary and Lu*, 1994]. This mechanism would complete a loop from equatorial SSTs through the atmosphere to midlatitude SSTs and then back through the ocean to equatorial SSTs. However, careful studies of Pacific SST variations in recent decades have shown that the oceanic pathway is ineffective because the midlatitude anomalies are diluted by mixing, especially as they move along the western boundary on their way to the equator [*Schneider et al.*, 1999]. Still, since subduction and advection of midlatitude waters are the ultimate source of the equatorial thermocline, this oceanic mechanism must become effective at some longer timescale, and alter the operation of the thermostat [*Hazeleger et al.*, 2001].

[45] Further, this study does not preclude the response of other components of the climate system independently capable of responding to external forcing (e.g., stratospheric ozone, the Atlantic meridional overturning circulation, monsoons). Indeed, ENSO could have been just part of a global response. Whether these subsystems acted in synergy will be left for future work. It is hoped that more complete models will soon be able to clarify their respective roles on such timescales.

6.3. Forcing Uncertainties

[46] Since the SST response to the moderate forcing ($\Delta F = 0.2\% S_o$) is just at the magnitude of the drought patterns of recent times [*Seager et al.*, 2005b], any reduction in the estimate of irradiance forcing makes the Sun an implausible cause of tropical Pacific climate change, let alone global climate change. So while there is a reasonably convincing empirical correspondence between proxies for solar output and tropical Pacific SSTs, the great uncertainties in solar irradiance forcing raise doubts about explanations of these SST variations as responses to solar forcing. Further, the hypothesis of a solar origin of millennial climate fluctuations is incumbent on the assumption that the corresponding signal in cosmogenic isotope records is indeed due to the Sun. We note that the most recent radiocarbon calibration effort, INTCAL04, displays weaker millennial cycles [*Reimer et al.*, 2004], though the production curve is still quite similar to INTCAL98, and such cycles are also present in a ^{10}Be record from Greenland [*Yiou et al.*, 1997]. In any event, their irradiance scaling may not be known with satisfactory accuracy for a long time. Amidst such an array of uncertainties, a useful inference can still be made: For moderate to strong scalings of solar variability, it is physically plausible that ocean-atmosphere feedbacks amplified those changes above the level of internal ENSO variability, but weak scalings are unable to produce the necessary changes.

[47] A major caveat, as stated before, is the absence of volcanic aerosol forcing in the present study. The results need to be reassessed once such a time series becomes available.

6.4. Theoretical Implications of a Solar-Induced ENSO-like Variability

[48] Our theory implies other predictions that should be testable with existing or future data:

6.4.1. Tropical Pacific SSTs

[49] Periods of increased solar irradiance should be more La Niña-like, in the absence of other radiative perturbations (e.g., volcanoes). The development of better reconstructions of solar irradiance, as well as high-resolution coral and sedimentary proxy records, will prove crucial for testing this hypothesis, during the past millennium and beyond.

6.4.2. Hemispheric Symmetry

[50] Tropical SSTs can influence midlatitudes and high latitudes via Rossby wave teleconnections [*Hoskins and Karoly*, 1981; *Horel and Wallace*, 1981] or the transient eddy response to SST-induced variations of subtropical jets [*Seager et al.*, 2003, 2005a]. Both cause climate anomalies with clear hemispheric symmetry. Consequently, if solar-induced ENSO variability did actually occur, it should appear in Southern Hemisphere climate records, e.g., tree ring records of drought-sensitive regions of South America. This is in contrast to the predictions of water-hosing experiments in the North Atlantic [*Zhang and Delworth*, 2005], which have asymmetric responses about the equator in the Pacific. It is hoped that high-resolution proxy data from the Southern Hemisphere will soon enable us to distinguish between these competing paradigms of global climate change.

7. Conclusions

[51] We propose that given a mid-to-high-range amplitude of Holocene solar irradiance variations, ENSO may have acted as one of the mediators between the Sun and the Earth's climate. The reasoning goes as follows: air/sea feedbacks amplified solar forcing to produce persistent, El Niño-like SST anomalies at times of decreased irradiance (the thermostat mechanism). In so doing, the ENSO system weakened the intensity of the Indian and Asian monsoons and triggered IRD discharge events in the North Atlantic, generating global climate variability on centennial to millennial timescales. It is likely that other feedbacks were involved in this process, such as the wind-driven and thermohaline circulation of the ocean and cloud feedbacks.

[52] So far, data from the past millennium and the longer Holocene seem to support our view. As more complete, and presumably more accurate, climate records become available, especially from the Southern Hemisphere, we hope that our mechanism can be tested in greater detail and on longer periods.

Appendix A

[53] We show evidence of a link between ENSO and surface winds over the northern North Atlantic. We use wind field data from three sources: surface observations, a coupled general circulation model (GCM), and a forced atmospheric GCM. The idea is to progressively strip down the physics to isolate the mechanism responsible for the linkage. We employed data from three sources:

[54] 1. The first is our best observational estimate of surface winds over the North Atlantic. Since wind stress estimates are unfortunately unavailable before 1949, the wind velocity field was taken from the analysis of *Evans and Kaplan* [2004], which uses an optimal interpolation (OI) of ICOADS winds (http://icoads.noaa.gov/) [*Worley et al.*, 2005]. This has the effect of retaining the large-scale features of the field, which are most relevant for our study.

[55] 2. The second is simulation H1 of the Geophysical Fluid Dynamics Laboratory (GFDL) coupled general circulation model (CM 2.1). This is a state-of-the-art ocean-atmosphere general circulation model in the configuration used for the Fourth Assessment report of the Intergovernmental Panel on Climate Change. The forcing is a reconstruction of natural and anthropogenic radiative perturbations over the period 1860–2000. This particular simulation has a vigorous, self-sustained ENSO with variance comparable to that observed. but very similar results were obtained with other ensemble members H2 and H3.

[56] 3. The third is a 16-member ensemble of simulations with the Community Climate Model (CCM3) model in POGA-ML (Pacific Ocean/Global Atmosphere) configuration, as used by *Seager et al.* [2005b]. The AGCM is coupled to a two-layer, entraining, mixed-layer ocean model, with historical SSTs [*Kaplan et al.*, 1998] prescribed only in the tropical Pacific (computed elsewhere). The results analyzed are the average of a 16-member ensemble, which isolates the influence of the boundary conditions, in this case, tropical Pacific SSTs over the period 1860–2000. The data can be found at http://kage.ldeo.columbia.edu:81/expert/SOURCES/.LDEO/.ClimateGroup/.MODELS/.CCM3/.PROJECTS/.poga-ML/.poga-ML-mean/. In both models we analyzed the wind stress, since it is the most relevant to surface ocean dynamics.

[57] The period of analysis was the longest common to all data sets, 1860–2000. All fields were smoothed by a 3-month running average. They were then regressed onto the corresponding NINO3 index: for historical SSTs, we used the extended SST analysis of *Kaplan et al.* [1998], while the model-generated NINO3 index was computed in the second example (GFDL H1).

[58] Results are shown in Figure 7 (left), which shows the regression patterns of surface wind stress (or velocity when analyses of stress were not available) on the normalized NINO3 index, and Figure 7 (right), which shows the linear correlation maps of the meridional component with NINO3. All data sets are in broad agreement that northeasterly winds tend to occur over the area of interest during periods of high NINO3. Nonetheless, the amplitudes are weak, and it is necessary to establish whether any of these correlations are statistically significant.

[59] For the period 1860–2000, with monthly data smoothed over 3-month intervals, $N \sim 500$, so the significance 95% threshold is $|\rho| \sim 0.1$. We found that correlations are significant at the 95% level everywhere in the POGA-ML ensemble mean (Figures 7c and 7d), which very effectively isolates the response to tropical SST variability. The correlation is consistently high in this case, because of a dynamical linkage between the two basins: the tropical warming due to El Niño displaces subtropical jets equatorward, modifying transient which induce equatorward low-level flow at high latitudes, with a noticeable zonally symmetric component [*Seager et al.*, 2003, 2005a]. In nature, however, this signal is potentially swamped by atmospheric dynamics independent of ENSO. Indeed, we find in the surface wind analyses (Figure 7f) that the ENSO/North Atlantic connection is very weak north of $\sim 48°N$. Repeating this analysis for five 50-year periods between 1860 and 2000 (sliding the window by 18 years each time), we found that this was due to a strong nonstationarity of the correlation in the northern parts of the basin: well above the 95% level in some decades, well below in some others. This result was also obtained for geostrophic wind fields derived from the sea level pressure (SLP) data of *Kaplan et al.* [2000]. This could be due either to observational error (in SST, winds, as well as SLP) or to noise. However, we found that a similar nonstationarity occurred in the GFDL simulations H1, H2, and H3, which have no measurement error. Therefore local variability is to blame in lowering the observed correlation to NINO3.

[60] This therefore suggests the following interpretation: A link between the tropical Pacific and the North Atlantic is at work in nature as in the two GCMs, but it is of modest amplitude compared to the natural climate variability of the North Atlantic, which is quite energetic in the multidecadal spectral range. The consequence is that the statistical link only emerges on long timescales. The simulated and instrumental SLP data are consistent with this idea, albeit too short to be conclusive, and perhaps veiled by the confounding influence of anthropogenic greenhouse gas increase.

References

Asmerom, Y., V. Polyak, S. Burns, and J. Rasmussen (2007), Solar forcing of Holocene climate: New insights from a speleothem record, southwestern United States, *Geology*, 35(1), 1–4, doi:10.1130/G22865A.1.

Bard, E., and M. Frank (2006), Climate change and solar variability: What's new under the sun?, *Earth Planet. Sci. Lett.*, 248(1–2), 1–14, doi:10.1016/j.epsl.2006.06.016.

Bard, E., G. Raisbeck, F. Yiou, and J. Jouzel (2000), Solar irradiance during the last 1200 years based on cosmogenic nuclides, *Tellus, Ser. B*, 52, 985–992.

Berger, A. L. (1978), Long term variations of daily insolation and Quaternary climatic changes, *J. Atmos. Sci.*, 35(12), 2362–2367.

Bjerknes, J. (1969), Atmospheric teleconnections from the equatorial Pacific, *Mon. Weather Rev.*, 97(3), 163–172.

Bond, G. (2005), Are Dansgaard-Oeschger cycles and multicentennial cycles of the Holocene and the last glacial interconnected?, *Geophys. Res. Abstr.*, *7*, SRef-ID:1607-7962/gra/EGU05-A-06038.

Bond, G., et al. (2001), Persistent solar influence on North Atlantic climate during the Holocene, *Science*, *294*(5549), 2130–2136.

Brönnimann, S., J. Luterbacher, J. Staehelin, T. M. Svendby, G. Hansen, and T. Svenoe (2004), Extreme climate of the global troposphere and stratosphere in 1940–42 related to El Niño, *Nature*, *431*, 971–974.

Brönnimann, S., E. Xoplaki, C. Casty, A. Pauling, and J. Luterbacher (2007), ENSO influence on Europe during the last centuries, *Clim. Dyn.*, *28*, 181–197, doi:10.1007/s00382-006-0175-z.

Bulic, I. H., and C. Brankovic (2006), ENSO forcing of the Northern Hemisphere climate in a large ensemble of model simulations based on a very long SST record, *Clim. Dyn.*, *28*, 231–254, doi:10.1007/s00382-006-0181-1.

Cane, M. A., and R. J. Patton (1984), A numerical-model for low-frequency equatorial dynamics, *J. Phys. Oceanogr.*, *14*(12), 1853–1863.

Chiang, J. C.H., M. Biasutti, and D. S. Battisti (2003), Sensitivity of the Atlantic Intertropical Convergence Zone to Last Glacial Maximum boundary conditions, *Paleoceanography*, *18*(4), 1094, doi:10.1029/2003PA000916.

Chung, C., and S. Nigam (1999), Asian summer monsoon—ENSO feedback on the Cane-Zebiak model ENSO, *J. Clim.*, *12*(9), 2787–2807.

Clement, A. C., R. Seager, M. A. Cane, and S. E. Zebiak (1996), An ocean dynamical thermostat, *J. Clim.*, *9*(9), 2190–2196.

Clement, A. C., R. Seager, and M. A. Cane (1999), Orbital controls on the El Niño/ Southern Oscillation and the tropical climate, *Paleoceanography*, *14*(4), 441–456.

Clement, A. C., R. Seager, and M. A. Cane (2000), Suppression of El Niño during the mid-Holocene by changes in the Earth's orbit, *Paleoceanography*, *15*(6), 731–737.

Cobb, K. M., C. D. Charles, H. Cheng, and R. L. Edwards (2003), El Niño/Southern Oscillation and tropical Pacific climate during the last millennium, *Nature*, *424*, 271–276.

Cook, E., C. Woodhouse, C. Eakin, D. Meko, and D. Stahle (2004), Long-term aridity changes in the western United States, *Science*, *306*(5698), 1015–1018, doi:10.1126/science.1102586.

Cook, E., R. Seager, M. Cane, and D. Stahle (2007), North American drought: Reconstructions, causes, and consequences, *Earth Sci. Rev.*, *81*(1–2), 93–134.

Crowley, T. J. (2000), Causes of climate change over the past 1000 years, *Science*, *289*(5477), 270–277.

Davis, M. (2001), *Late Victorian Holocausts: El Niño Famines and the Making of the Third World*, 464 pp., Verso, New York.

Eddy, J. (1977), Climate and the changing Sun, *Clim. Change*, *1*(2), 173–190.

Evans, M. N., and A. Kaplan (2004), The Pacific sector Hadley and Walker circulations in historical marine wind analyses, in *The Hadley Circulation: Present, Past and Future*, edited by H. F. Diaz and R. Bradley, pp. 239–258, Kluwer Acad., New York.

Fleitmann, D., S. J. Burns, M. Mudelsee, U. Neff, J. Kramers, A. Mangini, and A. Matter (2003), Holocene forcing of the Indian monsoon recorded in a stalagmite from southern Oman, *Science*, *300*(5626), 1737–1739, doi:10.1126/science.1083130.

Foukal, P., C. Frohlich, H. Spruit, and T. M. L. Wigley (2006), Variations in solar luminosity and their effect on the Earth's climate, *Nature*, *443*, 161–166, doi:10.1038/nature0507.

Fröhlich, C., and J. Lean (2004), Solar radiative output and its variability: Evidence and mechanisms, *Astron. Astrophys. Rev.*, *12*, 273–320.

Geller, M., and J. Alpert (1980), Planetary wave coupling between the troposphere and the middle atmosphere as a possible Sun-weather mechanism, *J. Atmos. Sci.*, *37*, 1197–1215.

Gill, A. E. (1980), Some simple solutions for heat-induced tropical circulations, *Q. J. R. Meteorol. Soc.*, *108*, 447–462.

Gupta, A., D. Anderson, and J. Overpeck (2003), Abrupt changes in the Asian southwest monsoon during the Holocene and their links to the North Atlantic Ocean, *Nature*, *421*, 354–357.

Haigh, J. D. (1996), The impact of solar variability on climate, *Science*, *272*(5264), 981–984.

Hazeleger, W., R. Seager, M. Visbeck, N. H. Naik, and K. Rodgers (2001), Impact of the midlatitude storm track on the upper Pacific Ocean, *J. Phys. Oceanogr.*, *31*(2), 616–636.

Herweijer, C., and R. Seager (2007), The global footprint of persistent extra-tropical drought in the instrumental era, *Int. J. Clim.*, in press.

Herweijer, C., R. Seager, and E. Cook (2006), North American droughts of the mid-to-late nineteenth century: A history, simulation and implication for mediaeval drought, *Holocene*, *16*(2), 159–171, doi:10.1191/0959683606hl917rp.

Herweijer, C., R. Seager, E. Cook, and J. Emile-Geay (2007), North American droughts of the last millennium from a gridded network of tree-ring data, *J. Clim.*, *20*, 1353–1376.

Hoerling, M. P., J. W. Hurrell, and T. Xu (2001), Tropical origins for recent North Atlantic climate change, *Science*, *292*(5514), 90–92.

Horel, J., and J. Wallace (1981), Planetary-scale atmospheric phenomena associated with the Southern Oscillation, *Mon. Weather Rev.*, *109*, 814–829.

Hoskins, B., and D. Karoly (1981), The steady linear response of a spherical atmosphere to thermal and orographic forcing, *J. Atmos. Sci.*, *38*, 1179–1196.

Jones, P. D., and M. E. Mann (2004), Climate over past millennia, *Rev. Geophys.*, *42*, RG2002, doi:10.1029/2003RG000143.

Kalnay, E., et al. (1996), The NCEP/NCAR 40-year Reanalysis Project, *Bull. Am. Meteorol. Soc.*, *77*, 437–471.

Kaplan, A., M. A. Cane, Y. Kushnir, A. C. Clement, M. B. Blumenthal, and B. Rajagopalan (1998), Analyses of global sea surface temperature 1856–1991, *J. Geophys. Res.*, *103*, 18,567–18,589.

Kaplan, A., Y. Kushnir, and M. Cane (2000), Reduced space optimal interpolation of historical marine sea level pressure: 1854–1992, *J. Clim.*, *13*(16), 2987–3002.

Karspeck, A., R. Seager, and M. A. Cane (2004), Predictability of tropical Pacific decadal variability in an intermediate model, *J. Clim.*, *18*, 2842–2850.

Koutavas, A., P. deMenocal, G. C. Olive, and J. Lynch-Stieglitz (2006), Mid-Holocene El Niño-Southern Oscillation (ENSO) attenuation revealed by individual foraminifera in eastern tropical Pacific sediments, *Geology*, *34*(12), 993–996.

Mann, M., and J. Lees (1996), Robust estimation of background noise and signal detection in climatic time series, *Clim. Change*, *33*, 409–445.

Mann, M. E., M. A. Cane, S. E. Zebiak, and A. Clement (2005), Volcanic and solar forcing of the tropical Pacific over the past 1000 years, *J. Clim.*, *18*(3), 447–456.

Marchal, O. (2005), Optimal estimation of atmospheric ^{14}C production over the Holocene: Paleoclimate implications, *Clim. Dyn.*, *24*(1), 71–88.

McCreary, J. P., and P. Lu (1994), Interaction between the subtropical and equatorial ocean circulations: The subtropical cell, *J. Phys. Oceanogr.*, *24*, 466–497.

Mordvinov, A., N. Makarenko, M. Ogurtsov, and H. Jungner (2004), Reconstruction of magnetic activity of the Sun and changes in its irradiance on a millennium timescale using neurocomputing, *Sol. Phys.*, *224*(1), 247–253.

Moy, C., G. Seltzer, D. Rodbell, and D. Anderson (2002), Variability of El Niño/Southern Oscillation activity at millennial timescales during the Holocene epoch, *Nature*, *420*, 162–165.

Muscheler, R., F. Joos, J. Beer, S. Muller, M. Vonmoos, and I. Snowball (2006), Solar activity during the last 1000 yr inferred from radionuclide records, *Quat. Sci. Rev.*, *26*, 82–97, doi:10.1016/j.quascirev.2006.07.012.

Neff, U., S. Burns, A. Mangini, M. Mudelsee, D. Fleitmann, and A. Matter (2001), Strong coherence between solar variability and the monsoon in Oman between 9 and 6 kyr ago, *Nature*, *411*, 290–293.

Pant, G. B., and B. Parthasarathy (1981), Some aspects of an association between the Southern Oscillation and Indian summer monsoon, *Arch. Meteorol. Geophys. Bioklimatol. Ser. B*, *29*, 245–251.

Peristykh, A. N., and P. E. Damon (2003), Persistence of the Gleissberg 88-year solar cycle over the last ∼12000 years: Evidence from cosmogenic isotopes, *J. Geophys. Res.*, *108*(A1), 1003, doi:10.1029/2002JA009390.

Rasmussen, E., and T. Carpenter (1982), Variations in tropical sea-surface temperature and surface winds associated with the Southern Oscillation/El Niño, *Mon. Weather Rev.*, *110*, 354–384.

Rasmussen, E. M., and T. H. Carpenter (1983), The relationship between eastern equatorial Pacific sea surface temperatures and rainfall over India and Sri Lanka, *Mon. Weather Rev.*, *111*, 517–528.

Reed, R. (1977), On estimating insolation over the ocean, *J. Phys. Oceanogr.*, *7*, 482–485.

Reimer, P., et al. (2004), INTCAL04 terrestrial radiocarbon age calibration, 0–26 cal kyr BP, *Radiocarbon*, *46*(3), 1029–1058.

Rein, B., A. Lückge, and F. Sirocko (2004), A major Holocene ENSO anomaly during the Medieval period, *Geophys. Res. Lett.*, *31*, L17211, doi:10.1029/2004GL020161.

Rind, D. (2002), The Sun's role in climate variations, *Science*, *296*(5568), 673–677.

Rind, D., D. Shindell, J. Perlwitz, J. Lerner, P. Lonergan, J. Lean, and C. McLinden (2004), The relative importance of solar and anthropogenic forcing of climate change between the Maunder Minimum and the present, *J. Clim.*, *17*(5), 906–929.

Rogers, J. C. (1984), The association between the North Atlantic Oscillation and the Southern Oscillation in the Northern Hemisphere, *Mon. Weather Rev.*, *112*(10), 1999–2015, doi:10.1175/1520-0493(1984)112.

Ropelewski, C., and M. Halpert (1987), Global and regional scale precipitation patterns associated with the El Niño/Southern Oscillation, *Mon. Weather Rev.*, *115*, 1606–1626.

Saint-Onge, G., J. S. Stoner, and C. Hillaire-Marcel (2003), Holocene paleomagnetic records from the St. Lawrence Estuary, eastern Canada: centennial- to millennial-scale geomagnetic modulation of cosmogenic isotopes, *Earth Planet. Sci. Lett.*, *209*, 113–130.

Schneider, N., A. J. Miller, M. A. Alexander, and C. Deser (1999), Subduction of decadal North Pacific temperature anomalies: Observations and dynamics, *J. Phys. Oceanogr.*, *29*, 1056–1070.

Schubert, S. D., M. J. Suarez, P. J. Pegion, R. D. Koster, and J. T. Bacmeister (2004), On the cause of the 1930s dust bowl, *Science*, *303*(5665), 1855–1859, doi:10.1126/science.1095048.

Seager, R., N. Harnik, Y. Kushnir, W. Robinson, and J. Miller (2003), Mechanisms of hemispherically symmetric climate variability, *J. Clim.*, *16*(18), 2960–2978.

Seager, R., N. Harnik, W. A. Robinson, Y. Kushnir, M. Ting, H. Huang, and J. Velez (2005a), Mechanisms of ENSO-forcing of hemispherically symmetric precipitation variability, *Q. J. R. Meteorol. Soc.*, *131*, 1501–1527, doi:10.1256/qj.04.n.

Seager, R., Y. Kushnir, C. Herweijer, N. Naik, and J. Velez (2005b), Modeling of tropical forcing of persistent droughts and pluvials over western North America: 1856–2000, *J. Clim.*, *18*(19), 4068–4091.

Shindell, D., D. Rind, N. Balachandran, J. Lean, and P. Lonergan (1999), Solar cycle variability, ozone, and climate, *Science*, *284*(5412), 305–308.

Shindell, D. T., G. A. Schmidt, M. E. Mann, D. Rind, and A. Waple (2001), Solar forcing of regional climate change during the Maunder Minimum, *Science*, *294*(5549), 2149–2152, doi:10.1126/science.1064363.

Shindell, D. T., G. A. Schmidt, R. L. Miller, and M. E. Mann (2003), Volcanic and solar forcing of climate change during the preindustrial era, *J. Clim.*, *16*, 4094–4107.

Stuiver, M., et al. (1998), INTCAL98 radiocarbon age calibration, 24000-0 cal BP, *Radiocarbon*, *40*(3), 1041–1084.

Thomson, D. J. (1982), Spectrum estimation and harmonic analysis, *Proc. IEEE*, *70*(9), 1055–1096.

Toniazzo, T., and A. Scaife (2006), The influence of ENSO on winter North Atlantic climate, *Geophys. Res. Lett.*, *33*, L24704, doi:10.1029/2006GL027881.

Torrence, C., and G. P. Compo (1998), A practical guide to wavelet analysis, *Bull. Am. Meteorol. Soc.*, *79*(1), 61–78.

Tudhope, A. W., et al. (2001), Variability in the El Niño-Southern Oscillation through a glacial-interglacial cycle, *Science*, *291*(5508), 1511–1516, doi:10.1126/science.1057969.

van Loon, H., and K. Labitzke (1988), Association between the 11-year solar cycle, the QBO, and the atmosphere. part ii: Surface and 700 mb in the Northern Hemisphere in winter, *J. Clim.*, *1*, 905–920.

Vellinga, M., and R. Wood (2002), Global climatic impacts of a collapse of the Atlantic thermohaline circulation, *Clim. Change*, *54*(3), 251–267.

Wagner, G., J. Beer, J. Masarik, R. Muscheler, P. Kubik, W. Mende, C. Laj, G. Raisbeck, and F. Yiou (2001), Presence of the solar De Vries cycle (∼205 years) during the last Ice Age, *Geophys. Res. Lett.*, *28*, 303–306.

Wang, Y., et al. (2005), The Holocene Asian monsoon: Links to solar changes and North Atlantic climate, *Science*, *308*(5723), 854–857, doi:10.1126/science.1106296.

Weber, S., T. Crowley, and G. van der Schrier (2004), Solar irradiance forcing of centennial climate variability during the Holocene, *Clim. Dyn.*, *22*(5), 539–553.

Worley, S. J., S. D. Woodruff, R. W. Reynolds, S. J. Lubker, and N. Lott (2005), Icoads release 2.1 data and products, *Int. J. Climatol.*, *25*(7), 823–842, doi:10.1002/joc.1166.

Yiou, F., et al. (1997), Beryllium 10 in the Greenland Ice Core Project ice core at Summit, Greenland, *J. Geophys. Res.*, *102*, 26,783–26,794.

Zebiak, S. E. (1982), A simple atmospheric model of relevance for El Niño, *J. Atmos. Sc.*, *39*, 2017–2027.

Zebiak, S. E., and M. A. Cane (1987), A model El Niño-Southern Oscillation, *Mon. Weather Rev.*, *115*(10), 2262–2278.

Zhang, R., and T. L. Delworth (2005), Simulated tropical response to a substantial weakening of the Atlantic thermohaline circulation, *J. Clim.*, *18*(12), 1853–1860.

————————————

P. Almasi, M. Cane, A. Kaplan, and R. Seager, Lamont-Doherty Earth Observatory of Columbia University, 61 Route 9W, P.O. Box 1000, Palisades, NY 10964-8000, USA.

J. Emile-Geay, Department of Earth and Atmospheric Sciences, Georgia Institute of Technology, E A S Office 2232, Ford ES&T, 311 Ferst Drive, Atlanta, GA 30332-0340, USA. (julien@gatech.edu)